

# 1      **Population Structure Discovery in Meta-Analyzed Microbial**

## 2      **Communities and Inflammatory Bowel Disease**

3      Siyuan Ma<sup>1,2</sup>, Dmitry Shungin<sup>2</sup>, Himmel Mallick<sup>1,2</sup>, Melanie Schirmer<sup>2</sup>, Long H. Nguyen<sup>3</sup>,

4      Raivo Kolde<sup>2</sup>, Eric Franzosa<sup>1,2</sup>, Hera Vlamakis<sup>2</sup>, Ramnik Xavier<sup>2\*</sup>, Curtis Huttenhower<sup>1,2\*</sup>

5      <sup>1</sup> Department of Biostatistics, Harvard T.H. Chan School of Public Health, Boston, MA, USA

6      <sup>2</sup> Broad Institute of MIT and Harvard, Cambridge, MA, USA

7      <sup>3</sup> Massachusetts General Hospital, Boston, MA, USA

## 8      **Abstract**

9      Microbial community studies in general, and of the human microbiome in inflammatory bowel  
10     disease (IBD) in particular, have now achieved a scale at which it is practical to associate features  
11     of the microbiome with environmental exposures and health outcomes across multiple large-scale  
12     populations. This permits the development of rigorous meta-analysis methods, of particular  
13     importance in IBD as a means by which the heterogeneity of disease etiology and treatment  
14     response might be explained. We have thus developed MMUPHin (Meta-analysis Methods with  
15     a Uniform Pipeline for Heterogeneity in microbiome studies) for joint normalization, meta-analysis,  
16     and population structure discovery using microbial community taxonomic and functional profiles.  
17     Applying this method to ten IBD cohorts (5,151 total samples), we identified a single consistent  
18     axis of microbial associations among studies, including newly associated taxa such as  
19     *Acinetobacter* and *Turicibacter* detected due to the sensitivity of meta-analysis. Linear random  
20     effects models further revealed associations with medications, disease location, and interaction  
21     effects consistent within and between studies. Finally, multiple unsupervised clustering metrics

22 and dissimilarity measures agreed on a lack of discrete microbiome “types” in the IBD gut  
23 microbiome. These results thus provide a benchmark for consistent characterization of the IBD  
24 gut microbiome and a general framework applicable to meta-analysis of any microbial community  
25 types.

## 26 **Introduction**

27 Meta-analysis for molecular epidemiology in large populations has seen great success in linking  
28 high-dimensional 'omic features to complex health-related phenotypes. One example of this is in  
29 genome-wide association studies (GWAS<sup>1</sup>), where the appropriate study scale, achieved by  
30 rigorous integration of multiple cohorts, has both facilitated reproducible discoveries (in the form  
31 of disease-associated loci<sup>2-4</sup>) and addressed confounding due to unobserved population  
32 structure<sup>5</sup>. The inflammatory bowel diseases (IBD) represent a particular success story for GWAS  
33 meta-analysis<sup>3,4</sup>, and environmental and microbial contributors complementing the condition's  
34 complex genetic architecture have been detailed by many individual studies<sup>6-8</sup>. However, in the  
35 absence of methods appropriate for large-scale microbial meta-analysis, the extent to which these  
36 findings reproduce across studies, or can be extended by increased joint sample sizes, remains  
37 undetermined. Likewise, it is unclear whether reproducible population structure in the microbiome,  
38 such as microbially-driven IBD “subtypes,” exists to help explain the clinical heterogeneity of these  
39 conditions<sup>9</sup>.

40 Meta-analysis of microbial community profiles presents unique quantitative challenges relative to  
41 other types of 'omics data such as GWAS<sup>10</sup> or gene expression<sup>11</sup>. These include particularly  
42 strong batch, inter-individual, and inter-population differences, and statistical issues including  
43 zero-inflation and compositionality<sup>12,13</sup>. Consequently, methods to correct for cohort and batch  
44 effects from other 'omics settings<sup>14-17</sup> are not directly appropriate. Two recent studies have  
45 suggested quantile normalization<sup>18</sup> and Bayesian Dirichlet-multinomial regression (BDMMA)<sup>19</sup> for

46 microbial profiles, which are applicable to a limited subset of differential abundance tests and do  
47 not provide batch-corrected profiles. To date, there are no methods permitting the joint analysis  
48 of batch-corrected microbial profiles for most study designs.

49 IBD represents one of the best-studied, microbiome-linked inflammatory phenotypes to date  
50 which thus stands to benefit from such approaches<sup>20,21</sup>. Among the inflammatory bowel diseases,

51 Crohn's disease (CD) and ulcerative colitis (UC) have been individually linked with structural and  
52 functional changes in the gut microbiome in many individual studies<sup>21</sup>. Each of CD and UC can  
53 itself be highly heterogeneous within the IBD population, however, and diversity in disease-  
54 associated gut microbial features has not been consistently associated with factors including  
55 disease subtype, progression, or treatment response<sup>7,9,22,23</sup>. Of note, two meta-analysis studies  
56 included IBD as one of several phenotypes<sup>24,25</sup>. These studies were not IBD-specific, did not have  
57 access to appropriate normalization techniques, nor took the aforementioned factors into account.

58 The complexity of microbial involvement in IBD<sub>1</sub> and the presence of substantial unexplained  
59 variation in the manifestation of its symptoms<sub>1</sub> makes it particularly appropriate for application of  
60 meta-analysis techniques.

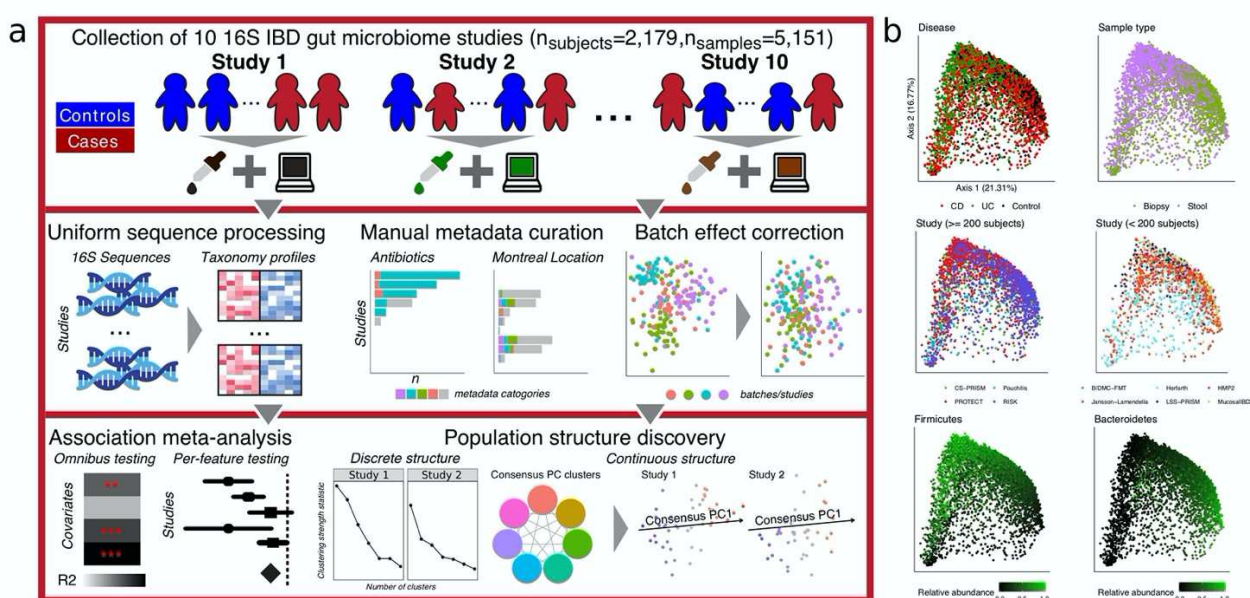
61 In this work, we introduce and validate a statistical framework for population-scale meta-analysis  
62 of microbiome data, and apply it to the largest collection to date of ten published 16S rRNA gene  
63 sequencing-based IBD studies (**Table 1**) to identify consistent disease associations and  
64 population structure. We found both previously documented and novel microbial links to the  
65 disease, with further differentiation among subtypes, phenotypic severity, and treatment effects.  
66 We further confidently conclude that there are no apparent, reproducible microbiome-based  
67 subtypes within CD or UC, which are instead a population structure gradient from less to more  
68 "pro-inflammatory" ecological configurations. Our work thus represents one of the first large-scale

69 efforts to assesses consistency in gut microbial findings for IBD and provides methodology  
70 supporting future microbial community meta-analyses.

71 **Results**

72 **Integrating 10 studies of the IBD stool and mucosal microbiomes**

73 We collected and uniformly processed ten published 16S studies of the IBD gut microbiome  
74 (**Table 1**, **Fig. 1a**, **Supplemental Table 1**) totaling 2,179 subjects and 5,151 samples. These  
75 studies range widely in terms of cohort designs and population characteristics, including recent-  
76 onset and established disease patients, cross-sectional and longitudinal sampling, pediatric and  
77 adult populations, diseases (CD and UC), treated and treatment-naïve patients, biopsy and stool  
78 samples, and inclusion of healthy/non-IBD controls. Covariates were manually curated to ensure  
79 consistency across studies (**Methods**). Major factors available from all or most studies included  
80 demographics (age/sex/race), biogeography, disease location and/or extent, antibiotic usage,  
81 immunosuppression, and steroid and/or 5-ASA usage.



83 **Figure 1: A method for large-scale microbial community meta-analysis and its application to inflammatory**  
84 **bowel disease. a)** We developed a novel statistical framework, MMUPHin, allowing joint normalization and meta-  
85 analysis of large microbial community profile collections with heterogeneous and complex designs (multiple covariates,  
86 longitudinal samples, etc.). We applied it to a collection of 10 inflammatory bowel disease studies comprising 2,179  
87 subjects and 5,151 total samples (**Table 1**). We uniformly processed the associated sequence data and harmonized  
88 metadata across cohorts. Microbial taxonomic profiles were then corrected for batch- and study-effects before  
89 downstream analyses for omnibus and per-feature association with disease phenotypes and unsupervised population  
90 structure discovery. **b)** MDS ordination of all microbial profiles (Bray-Curtis dissimilarity) before batch correction  
91 visualize the strongest associations with gut microbial composition, including disease, sample type (biopsy or stool),  
92 cohort (visualized separately for larger and smaller studies), and dominant phyla.

93 Using this joint dataset and upon uniform bioinformatics processing (**Methods**), we first assessed  
94 the factors that corresponded to overall variation in microbiome structure, which included disease  
95 status, sample type (biopsy versus stool), and dominant phyla (Bacteroidetes and Firmicutes, **Fig.**  
96 **1b**). Cohort effects prior to batch correction and meta-analysis were also significant. Microbiome  
97 differences associated with disease were notable even without normalization. However, this can  
98 be misleading due to the confounding of cohort structure between studies, such as the  
99 differentiation between RISK (a predominantly mucosal study of CD) and PROTECT (a  
100 predominantly stool study of UC). Inter-individual differences largely independent of population or  
101 disease, such as Bacteroidetes versus Firmicutes dominance, were also universal among studies  
102 and sample types as expected<sup>9,26</sup>. Many of these factors were of comparable effect size, both  
103 visually and as quantified below, emphasizing the need for covariate-adjusted statistical modelling  
104 to delineate the biological (disease, treatment) and technical (cohort, batch) effects associated  
105 with individual taxa throughout the cohorts (**Supplemental Notes**, **Supplemental Fig. 1-3**).

Study	Brief description	N subject	N sample	Phenotype(s)	Age	Gender	Sample type(s)
PROTECT <sup>23</sup>	Longitudinal cohort of newly diagnosed UC	405	1212 (539)	UC 405	12.71 (3.29)	Male 52%/ Female 48%	Biopsy 22%/ Stool 78%

RISK <sup>7</sup>	Pediatric cohort of treatment-naïve CD	631	882	CD 430/ Control 201	12.16 (3.22)	Male 59%/ Female 41%	Biopsy 72%/ Stool 28%
Herfarth <sup>7</sup>	Densely (daily) sampled longitudinal cohort	31	860 (31)	CD 19/ Control 12	36.03 (14.12)	Male 35%/ Female 58%/ Missing 6%	Stool
Jansson-Lamende Ila <sup>22</sup>	Longitudinal follow up with fecal samples	137	683 (137)	CD 49/ UC 60/ Control 28		Male 42%/ Female 58%	Stool
Pouchitis <sup>28</sup>	Patients recruited underwent IPAA for treatment of UC or FAP prior to enrollment.	353	577	CD 42/ UC 266/ Control 45	46.19 (13.58)	Male 52%/ Female 48%	Biopsy
CS-PRISM <sup>29</sup>	Cross sectional cohort nested in PRISM	397	467	CD 215/ UC 144/ Control 38	41.68 (15.22)	Male 47%/ Female 53%	Biopsy 29%/ Stool 71%
HMP <sup>9</sup>	Large cohort of newly diagnosed IBD with multi 'omics measurement.	81	177 (162)	CD 37/ UC 22/ Control 22	29.76 (19.63)	Male 51%/ Female 49%	Biopsy
Mucosall BD <sup>30</sup>	Pediatric cohort with Paneth cell phenotypes	83	132	CD 36/ Control 47	12.93 (3.65)	Male 58%/ Female 42%	Biopsy
LSS-PRISM <sup>31</sup>	Longitudinal cohort nested in PRISM.	18	88 (19)	CD 12/ UC 6	30.37 (10.52)	Male 39%/ Female 61%	Stool
BIDMC-FMT <sup>32</sup>	FMT Trial design	8	16	CD 8	38.38 (12.73)	Male 62%/ Female 38%	Stool

106 **Table 1: 10 uniformly processed 16S rRNA gene sequencing studies of the IBD mucosal/stool microbiomes.**

107 For longitudinal cohorts, numbers in parentheses indicate baseline sample size. For age, mean and standard error  
108 (parenthesized) are shown. Additional covariates are summarized in **Supplemental Table 1**.

109 **A statistical framework for meta-analysis of microbial community profiles**

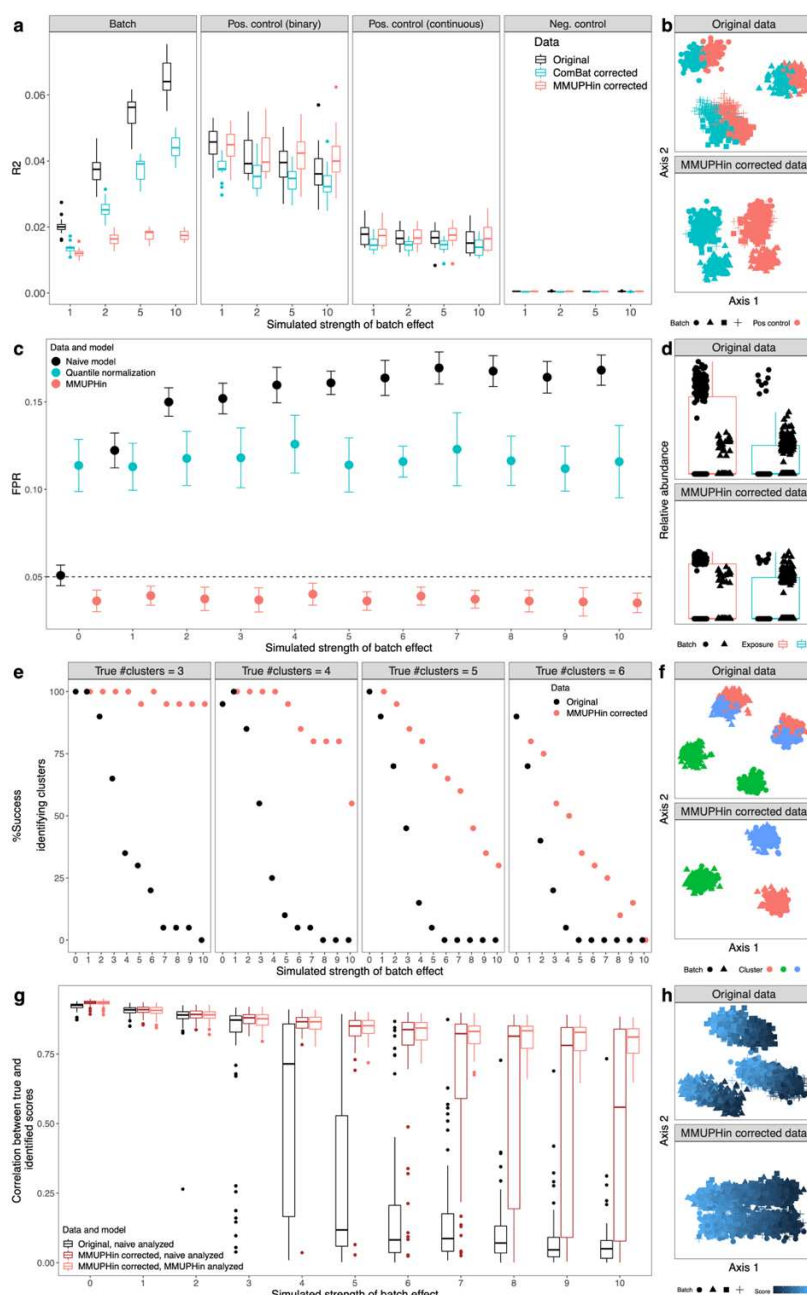
110 We developed a collection of novel methods for meta-analysis of environmental exposures,  
111 phenotypes, and population structures across microbial community studies, specifically  
112 accounting for technical batch effects and interstudy differences (**Methods, Fig. 1a**). It consists  
113 of three main components: batch and study effect correction, covariate modeling, and population  
114 structure discovery. First, we extended methods from the gene expression literature (ComBat<sup>15</sup>)  
115 to enable batch correction of zero-inflated microbial abundance data. Based on linear modelling,  
116 the method can differentiate between technical effects (batch, study) versus covariates of  
117 biologically interest (exposure, phenotype). Second, we combined well-validated data  
118 transformation and linear modelling combinations for microbial community profiles<sup>33</sup> with fixed and  
119 random effect modelling<sup>34</sup> for meta-analytical synthesis of per-feature (taxon, gene, or pathway)  
120 differential abundance effects. Lastly, we generalized and formalized approaches from cancer  
121 transcriptional subtyping<sup>35</sup> to permit unsupervised discovery and validation of both discrete and  
122 continuous population structures in microbial community data (**Supplemental Fig. 4**). Our  
123 methods, implemented as Meta-analysis Methods with a Uniform Pipeline for Heterogeneity in  
124 microbiome studies (MMUPHin), are available as an R package through Bioconductor<sup>36</sup> and at  
125 <https://bioconductor.org/packages/release/bioc/html/MMUPHin.html>.

126 We validated MMUPHin both in comparison to existing methods and through extensive simulation  
127 studies (**Fig. 2**), with simulated realistic microbial abundance profiles at different data  
128 dimensionality, biological/technical batch signal strength, and discrete/continuous population  
129 structures (**Methods, Supplemental Table 2, Supplemental Fig. 5-8**). MMUPHin successfully  
130 reduced variability attributable to technical effects in simulated microbial profiles, as first quantified

131 by the PERMANOVA R2 statistic<sup>37</sup> (**Fig. 2a-b, Supplemental Fig. 5**). This was true both in terms  
132 of reducing the overall microbial variability attributable to technical artifacts and in terms of the  
133 ratio of “biological” versus technical variability (**Fig. 2a**). ComBat correction<sup>15</sup>, suited for gene  
134 expression data, was capable of reducing batch effects to a lesser degree, but also tended to  
135 reduce desirable “biological” variation in the process, likely due to noise introduced by it changing  
136 many zero counts to non-zero values. Previously proposed techniques for microbial community  
137 data, namely quantile normalization<sup>18</sup> and BDMMA<sup>19</sup>, are only appropriate for differential  
138 abundance analysis and do not provide batch-normalized profiles, thus precluding PERMANOVA  
139 batch effect quantification; their per-feature testing performance is evaluated together with  
140 MMUPHin in the following section. MMUPHin thus provides batch-corrected microbial community  
141 profiles that retain biologically meaningful variation more than (or not even possible using) existing  
142 methods.

143 For differential abundance testing, MMUPHin successfully corrected for false associations when  
144 batch/cohort effects were confounded with variables of interest, which is a common concern for  
145 ‘omics meta-analysis<sup>38</sup>, while quantile normalization<sup>18</sup> and BDMMA<sup>19</sup> had either inflated or overly  
146 conservative false positive rates (**Fig. 2c-d, Supplemental Fig. 6**). We also validated MMUPHin’s  
147 support for unsupervised population structure discovery, in addition to these “supervised”  
148 differential abundance and statistical association tests. In microbial communities, valid,  
149 generalizable population structure can manifest as either discretely clustered subtypes<sup>39</sup> or as  
150 continuously variable gradients of community configurations<sup>40</sup>, but methods for discovery are  
151 particularly susceptible to false positives in the presence of technical artifacts<sup>26,40</sup>. To this end, for  
152 discrete structures, MMUPHin utilizes established clustering strength evaluation metrics<sup>41</sup> to a)  
153 evaluate the existence of discrete clusters within individual microbiome studies and b) to validate  
154 the reproducibility of such structures among studies meta-analytically (**Fig. 2e-f, Supplemental**  
155 **Fig. 7**). For continuous structures, our method generalizes single study principal component

156 analysis (PCA<sup>42</sup>) to multiple studies by constructing a network of correlated top PC loadings<sup>35</sup>,  
 157 thus identifying major axes of variation that explain the largest amount of heterogeneity between  
 158 microbial profiles and are also consistent across studies (**Fig. 2g-h, Supplemental Fig. 8**). As a  
 159 result, MMUPHin was able to successfully identify discrete clusters (i.e. microbiome "types") when  
 160 present, as well as significantly consistent continuous patterns of microbiome variation that recur  
 161 among populations (**Supplemental Notes**).

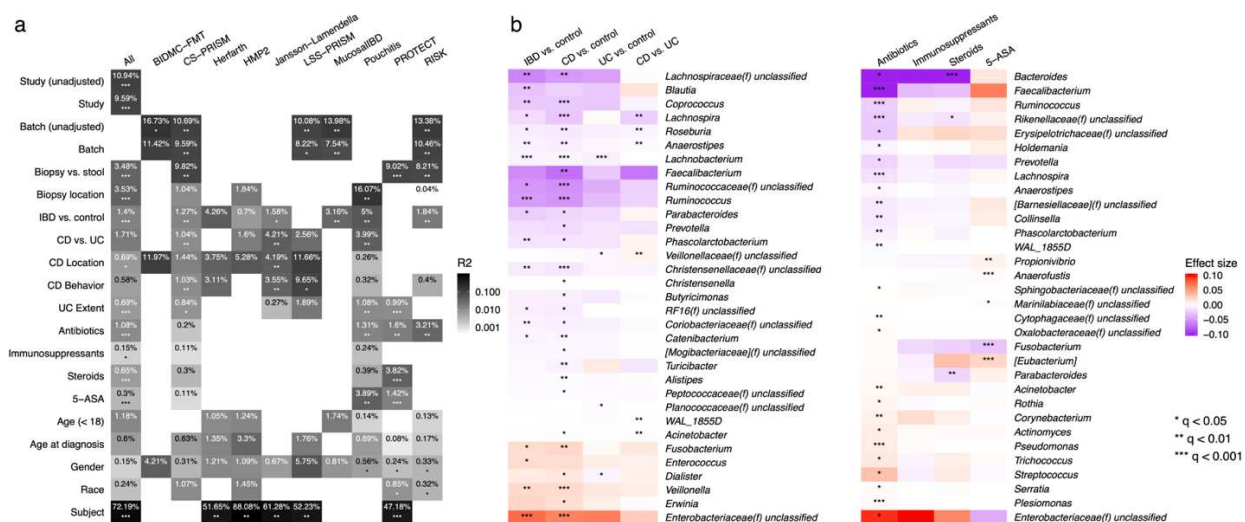


163 **Figure 2: Effectiveness of batch correction, association meta-analysis, and unsupervised population structure**  
164 **discovery methods.** All evaluations use simulated microbial community profiles as detailed in Methods. Left panels  
165 summarize representative subsets of results (full set of simulation cases presented in **Supplemental Table 2** and  
166 results in **Supplemental Fig. 5-8**), and right panels show examples of batch-influenced data pre- and post-correction.  
167 a, b) MMUPHin is effective for covariate-adjusted batch effect reduction while maintaining the effect of positive control  
168 variables. Results shown correspond to the subset of details in **Supplemental Fig. 5** with number of samples per batch  
169 = 500, number of batches = 4, and number of features = 1000 with 5% spiked with associations. c, d) Batch correction  
170 and meta-analysis reduces false positives when an exposure is spuriously associated with microbiome features due to  
171 an imbalanced distribution between batches. Corresponds to **Supplemental Fig. 6** with number of samples per batch  
172 = 500, number of features = 1000 with 5% spiked associations, and case proportion difference between batches = 0.8.  
173 Evaluations of BDMMA generates low FPRs due to the zero-inflated nature of simulated microbial abundances, and  
174 are included only in **Supplemental Fig. 6**. e, f) Batch correction improves correct identification of the true underlying  
175 number of clusters during discrete population structure discovery. Corresponds to **Supplemental Fig. 7** with number  
176 of batches = 4. g, h) Continuous structure discovery accurately recovers microbiome compositional gradients in a  
177 simulated population. Corresponds to **Supplemental Fig. 8** with number of batches = 6.

178 **Meta-analysis of the IBD microbiome**

179 Given these validations of MMUPHin's accuracy in simulated data, we next applied it to the 10-  
180 study, 4,789-sample IBD gut amplicon profile meta-analysis introduced above (**Fig. 3**). MMUPHin  
181 successfully reduced the effects both of differences among studies, and of batches within studies  
182 (study effect correction modelling disease and sample type as covariates, see **Methods**),  
183 although these remained among the strongest source of variation among taxonomic profiles as  
184 quantified by PERMANOVA R2 (**Fig. 3a, Methods, Supplemental Table 3**). Among biological  
185 variables, sample type (biopsy/stool), biopsy location (multiple, conditional on biopsy samples),  
186 disease status (IBD/control), and disease types (CD/UC, conditional on IBD) consistently had the  
187 strongest effect on the microbiome among studies. Several relationships between study design  
188 and phenotypic effects were apparent. Batches had a particularly strong effect in CS-PRISM and  
189 RISK, for example, where biopsy and stool samples were also perfectly separated by batch.

190 Treatment exposures all had small effects on microbiome structure within studies, which typically  
 191 reached statistical significance only when combined by meta-analysis; antibiotics were an  
 192 exception with slightly larger effects. Montreal classification did not generally correspond with  
 193 significant variation, while age (at sample collection as stratified below and above 18, and at  
 194 diagnosis by Montreal age classification<sup>43</sup>) had small but significant effects. The effects of gender  
 195 and race were not significant. Lastly, for longitudinal studies, relatively stable differences between  
 196 subjects over time were large and significant, consistently for both longer-interval (HMP2) as well  
 197 as densely sampled cohorts (Herfarth, daily samples), in agreement with previous individual  
 198 studies' observations<sup>9,23</sup>.



199 **Figure 3: Meta-analytic omnibus and per-feature testing reveal novel and previously documented IBD associations.** a) Omnibus testing (PERMANOVA on Bray-Curtis dissimilarities with stratification and covariate control where appropriate, see **Methods** and **Supplemental Table 3**) identified between-subject differences as the greatest source of microbiome variability, with IBD phenotype, disease (CD/UC), and sample type (stool/biopsy) as additional main sources of biological variation. MMUPHin successfully reduced between-cohort and within-study batch effects, although these technical sources also remained significant contributors to variability. b) Individual taxa significantly associated with IBD phenotypes or treatments after meta-analysis. Taxa are arranged by family-level median effect size of IBD vs. control for disease results and that of antibiotic usage for treatment results. Effect sizes are aggregated regression coefficients (across studies with random effects modelling) on arcsin square root-transformed relative

209 abundances. Detailed model information in **Methods** and **Supplemental Table 3**. Individual study results in  
210 **Supplemental Table 4**.

211 We identified individual taxonomic features consistently associated with disease and treatment  
212 variables (**Fig. 3b, Supplemental Table 4**), with meta-analysis multivariate differential  
213 abundance analysis, adjusting for common demographics (age, gender, race) and further  
214 stratifying for sample type and disease when appropriate (**Methods, Supplemental Table 3**). At  
215 a very high level, differential abundance patterns between CD and control microbiomes were  
216 consistent with, and often more severe than contrasts between UC and control, confirming with  
217 increased resolution previous observations that CD patients tend to have more aggravated  
218 dysbiosis than UC patients<sup>9</sup>. As expected, our meta-analysis confirms many of the taxa  
219 associated with IBD reported by previous individual (**Fig. 3b**, detailed in **Supplemental Notes**);  
220 these findings strongly supports the emerging hypotheses of pro-inflammatory aerotolerant  
221 clades forming a positive feedback loop in the gut during inflammation, often of oral origin<sup>7</sup>, and  
222 depleting the gut's typical fastidious anaerobe population as a result.

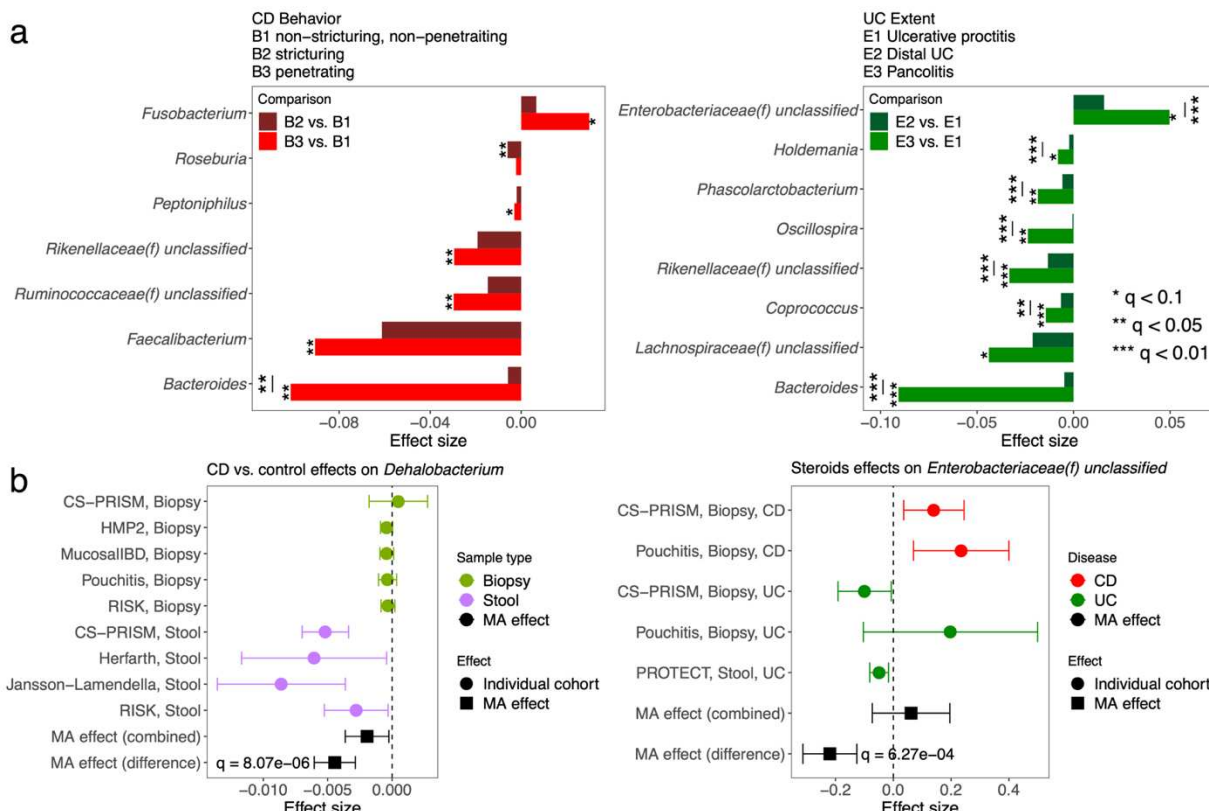
223 We also identified two taxa not previously associated with IBD, both of modest effect sizes and  
224 likely newly detected by the meta-analysis' increased power. The genus *Acinetobacter* was  
225 enriched in CD, and *Turicibacter* was depleted. *Turicibacter* in particular is poorly represented in  
226 reference sequence databases, with only nine genomes for one species (*Turicibacter sanguinis*)  
227 currently in the NCBI genome database; this makes it easy to overlook in shotgun metagenomic  
228 profiles relative to amplicon sequencing. The genus *Acinetobacter*, conversely, is quite well  
229 characterized due to its role in antimicrobial resistant infections<sup>44</sup>, and it was previously linked  
230 specifically to the primary sclerosing cholangitis phenotype in UC<sup>45</sup>, although without follow-up to  
231 our knowledge. *Turicibacter* is overall less characterized both in isolation and with respect to  
232 disease, although our findings and others' suggest it might be inflammation-sensitive when  
233 present; it was one of many clades increased in mice during CD8+ T cell depletion<sup>46</sup> and reduced

234 in a homozygous TNF deletion<sup>47</sup>. As the strains of *Acinetobacter* implicated in gut inflammation  
235 are unlikely to be those responsible for e.g. nosocomial infections, further investigation of both  
236 clades using more detailed data or IBD-specific isolates is warranted.

237 Among treatment variables (samples or time points during which subjects were receiving  
238 antibiotics, immunosuppressants, steroids, and/or 5-ASAs), antibiotics had the strongest effects  
239 on individual taxa, as well as the greatest number of significantly associated taxa (**Fig. 3b**). These  
240 associations are also broadly in agreement with previous observations for microbiome responses  
241 to antibiotics in IBD or generally, e.g. the depletion of *Faecalibacterium*, *Ruminococcus*, and  
242 *Bacteroides* in patients treated with antibiotics, and the enrichment of (often stereotypically  
243 resistant) taxa such as *Streptococcus*, *Acinetobacter*, and the Enterobacteriaceae, with  
244 differential responses to the treatment groups speaking to both administration considerations and  
245 their impact on host versus microbial community bioactivities (**Supplemental Notes**).

246 Subsets of IBD-linked taxa were additionally associated with the diseases' phenotypic severity  
247 (**Fig. 4a, Supplemental Table 5**). Montreal classification<sup>43</sup> was used as a proxy for disease  
248 severity, including Behavior categories for Crohn's disease (B1 non-stricturing, non-penetrating,  
249 B2 stricturing, non-penetrating, B3 stricturing and penetrating) and Extent for ulcerative colitis (E1  
250 limited to rectum, E2 up to descending colon, E3 pancolitis). We tested for features differentially  
251 abundant in the more severe phenotypes when compared against the least severe category (B1  
252 CD and E1 UC, **Methods**). Among statistically significant results, many extended those identified  
253 above as overall IBD associated (**Fig. 3b**), such as the depletion of *Faecalibacterium* in B3 CD  
254 and *Roseburia* in B2 CD, as well as the enrichment of Enterobacteriaceae in E3 UC. In most  
255 cases, microbial dysbiosis was also additionally aggravated from the moderate to the most  
256 extreme disease manifestations; such differences were statistically significant (**Methods**) in, for  
257 example, the progressive depletion of *Bacteroides* in CD and UC, as well as the enrichment of  
258 Enterobacteriaceae in UC. This meta-analysis is uniquely powered to detect these subtle

259 differences, which aid in shedding light on the microbiome's response to progressive inflammation  
 260 and disease subtypes. Pancolitis corresponds with a unique microbial configuration distinct from  
 261 regional colitis and not generally detectable in smaller studies<sup>6</sup>, for example, while more severe  
 262 CD induces essentially a more extreme form of the same dysbiosis observed in less severe forms  
 263 of the disease.



264

265 **Figure 4: IBD-associated taxa are aggravated in more severe disease; disease biogeography and CD/UC**  
 266 **differentially affect some taxa with respect to disease and treatment.** a) Statistically significant genera from meta-  
 267 analytically synthesized differential abundance effects among severity of CD and UC phenotypes as quantified by  
 268 Montreal classification. The difference between the most severe phenotype with the least severe one (B3 vs. B1 for  
 269 CD, E3 vs. E1 for UC) was in most cases more aggravated than that of the intermediate phenotype. Many of the  
 270 identified features overlap with those associated with IBD vs. control differences, suggesting a consistent gradient of  
 271 severity effects on the microbiome. Individual study results in **Supplemental Table 5**. b) Genus *Dehalobacterium* as  
 272 an example in which a taxon is uniquely affected in the stool microbiome during CD and not at the mucosa. Likewise,  
 273 family Enterobacteriaceae as an example in which steroid treatment corresponds with enrichment of the clade in CD

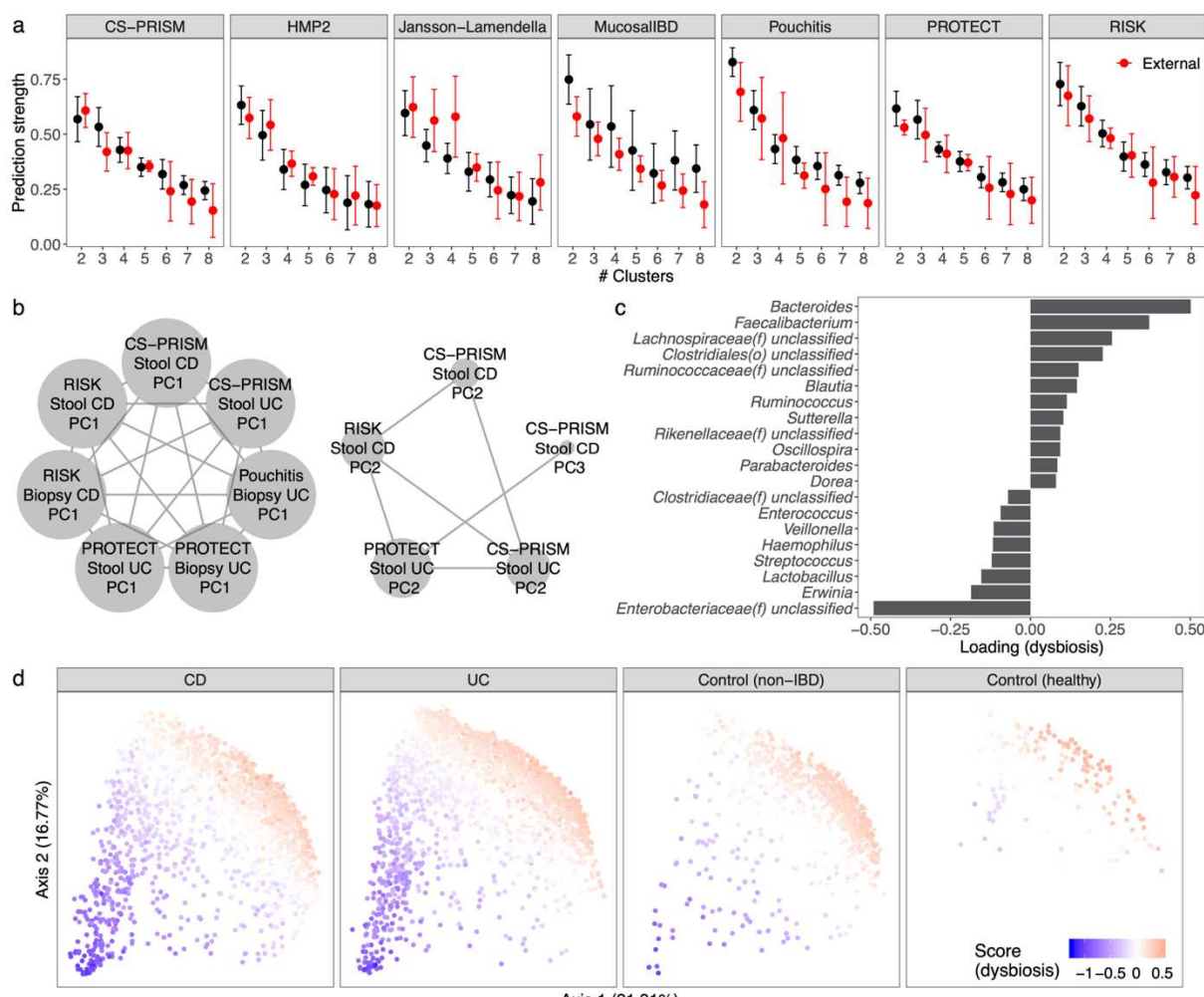
274 samples, but depletion in UC. In all panels, effect sizes are aggregated regression coefficients on arcsin square root-  
275 transformed relative abundances. Full sets of statistically significant interactions, with individual study results, are in  
276 **Supplemental Table 6**.

277 Additionally, diseases (CD and UC) and their corresponding dysbioses also interacted distinctly  
278 with the microbiome under different treatment regimes and in different biogeographical  
279 environments (mucosa vs. stool, **Fig. 4b, Supplemental Table 6**). Interaction effects, in the  
280 statistical sense, were defined as a main exposure (IBD or treatment) having differential effects  
281 on taxon abundance with respect to either sample type (biopsy/stool) or diseases (CD/UC); they  
282 were identified via moderator meta-analysis models (**Methods**). Overall, we found elevated  
283 effects of both CD (relative to controls) and antibiotic treatment in stool as compared to biopsy-  
284 based measurements of the microbiome (**Supplemental Table 6**). An example of this is  
285 *Dehalobacterium*, with significantly greater depletion in CD stool relative to biopsies (**Fig. 4b**).  
286 *Dehalobacterium*, as with *Turicibacter* above, is underrepresented in reference sequence  
287 databases, better-detected by amplicon sequencing, and thus not a common microbial signature  
288 of IBD. It has been linked to CD in at least one existing 16S-based stool study<sup>48</sup>. In contrast,  
289 several UC-specific microbial disruptions were more prominent at the mucosa (i.e. in biopsies,  
290 **Supplemental Table 6**). Coupled with the severity-linked differences above, this suggests CD-  
291 induced changes in the entire gut microbial ecosystem largely as a consequence of inflammation,  
292 with UC-induced dysbioses both more local and more specific to disease and treatment regime.  
293 Additional results include effect of steroids on the Enterobacteriaceae, which tended to be more  
294 abundant in CD patients receiving steroids, but less abundant in UC recipients (**Fig. 4b**,  
295 **Supplemental Table 6, Supplemental Notes**).

296 **Consistent IBD microbial population structure discovered by unsupervised analysis**

297 The existence of subtypes within gut microbial communities has been a major open question in  
298 human microbiome studies, and it is of particular importance within IBD as a potential explanation

299 for heterogeneity in disease etiology and treatment response<sup>6,9</sup>. To systematically characterize  
300 population structure in the IBD gut microbiome that was reproducible among studies, we  
301 performed both discrete and continuous structure discovery on the 10 cohorts using our meta-  
302 analysis framework. To identify potential discrete community types (i.e. clusters), we performed  
303 clustering analysis within each cohort's IBD patient population, and evaluated the clustering  
304 strength via prediction strength (**Methods**). We found no evidence to support discrete clustering  
305 structure within individual cohorts, nor were we able to reproduce each cohort's clustering results  
306 externally (**Fig. 5a**). This lack of discrete structure was consistent when we further stratified  
307 samples to either CD or UC populations (**Supplemental Fig. 9**), or extended to additional  
308 dissimilarity metric and clustering strength measurements (**Supplemental Fig. 9, Methods**). Our  
309 observation that the IBD gut microbiome cannot be well characterized by discrete clusters is thus  
310 consistent with previous findings on gut microbial heterogeneity for healthy populations<sup>40</sup> and  
311 suggests that, at the level powered by this study, such microbiome subtypes are not clearly  
312 responsible for clinical heterogeneity.



313

314 **Figure 5: Unsupervised population structure discovery finds no evidence of microbiome-based subtypes in**  
 315 **the IBD gut, but a reproducible gradient of continuously variable dysbiosis in disease. a)** No support was  
 316 detected for discrete microbiome subtypes (clusters) within the IBD microbiome, neither within cohort nor when  
 317 evaluated among studies (red bars) using prediction strength<sup>41</sup>. This remained true during stratification within CD and  
 318 UC, and for additional dissimilarity metric/clustering strength measurements (**Supplemental Fig. 9**). **b)** Conversely,  
 319 two reproducible, continuously variable patterns of microbiome population structure were identified using groups of  
 320 similar principal components (**Methods**)<sup>35</sup>. These patterns were consistent within and between cohorts, disease types,  
 321 and sample types, as well as under different edge strength cutoffs (**Supplemental Fig. 11**), and their consensus  
 322 loadings were reproducible among cohorts (**Supplemental Fig. 12**). **c)** Top 20 genera with highest absolute loadings  
 323 for the disease-associated dysbiosis score corresponding to the first cluster in **b**. Many of these taxa were also IBD-  
 324 associated (**Fig. 3b**). **d)** Distribution of the dysbiosis pattern across CD, UC, non-IBD control, and healthy populations.

325 Although it was defined in an unsupervised way solely within the IBD population, across which the pattern is highly  
326 variable, it also differentiates well between IBD and control populations (**Supplemental Fig. 13**).

327 Conversely, we identified two consistent, continuously varying gradients of microbial community  
328 variation in the IBD microbiome (**Fig. 5b-d, Supplemental Fig. 10**). These gradients represent  
329 patterns of microbes that occur with greater or lesser abundance in tandem, and which covary  
330 across subjects in a population; they were identified as principal component (PC) vectors that  
331 recur among different cohorts (see **Methods**)<sup>35</sup>. Briefly, we used the four largest IBD cohorts (CS-  
332 PRISM, Pouchitis, PROTECT, and RISK) as training datasets to identify two clusters of consistent  
333 PCs (**Fig. 5b**), which were confirmed with sensitivity analysis (**Supplemental Fig. 11**) and  
334 validated in the remaining cohorts (**Supplemental Fig. 12**). The consensus loadings (i.e. within-  
335 cluster average) representing these two clusters (**Fig. 5c, Supplemental Fig. 10, Supplemental**  
336 **Table 7**) were used to assign continuously varying scores to the IBD population that capture  
337 gradient changes in the microbiome that occurred consistently within IBD, across diseases,  
338 sample types, and cohorts. This disease-linked "type" of microbiome variation corresponded  
339 roughly to severity or extent of inflammation, as detailed below.

340 In particular, while the second continuous population structure captured the Firmicutes-  
341 Bacteroidetes tradeoff present in most gut microbiome studies (**Supplemental Fig. 10**)<sup>9,26,40</sup>, the  
342 first continuous score was IBD-specific and corresponded roughly to more extreme disease-  
343 associated dysbiosis in CD and UC populations (**Fig. 5d**). This is evidenced by the taxa with  
344 highest weights in the scores' consensus loading vector (**Fig. 5c**), which included taxa  
345 differentially abundant between IBD and control populations (**Fig. 3**). The score was consistent  
346 both within CD and UC while also further differentiating IBD, non-IBD control, and healthy  
347 populations (**Fig. 5d, Supplemental Fig. 13**), even though it was identified unsupervisedly only  
348 from diseased subsets. The composition of the score and its population structure are also  
349 consistent with our recent definition of dysbiotic gut microbiome configurations corresponding with

350 multi'omic perturbations during IBD activity<sup>9</sup>. Together with the supervised meta-analysis results  
351 above, these unsupervised population structure findings confirm that there are no detectable  
352 discrete subtypes of the gut microbiome in IBD even among ~5,000 combined samples, while  
353 showing a single continuously variable gradient of microbiome changes reproducibly present  
354 during more dysbiotic diseases.

## 355 **Discussion**

356 Here, we provide a novel framework for microbial community meta-analysis and apply it to the  
357 first large-scale integration of over 5,100 amplicon profiles of the stool and mucosal microbiomes  
358 in IBD. This identified a significantly reproducible gradient in the gut microbiome indicative of  
359 increasing dysbiosis in subsets of patients. The study also showed no evidence of additional  
360 population structure, such as microbiome-driven discrete disease subtypes, within CD or UC. The  
361 increased power provided by meta-analysis supported many of the taxonomic associations  
362 previously ascribed to IBD (e.g. *Faecalibacterium*, *Ruminococcus*, Enterobacteriaceae) while  
363 uncovering new associations (*Turicibacter*, *Acinetobacter*) not confidently associated with  
364 inflammation by other populations or data types. Almost all effects were exhibited similarly using  
365 either stool or mucosal profiling, with a small number of exceptions showing significant  
366 differentiation (e.g. *Dehalobacterium*). Novel disease-treatment response interactions were  
367 observed (e.g. steroids on Enterobacteriaceae). Finally, the meta-analysis framework developed  
368 for the study, MMUPHin, has been extensively evaluated and its performance for batch effect  
369 removal, supervised meta-analysis of exposures and covariates, and unsupervised population  
370 structure discovery validated on a variety of simulated microbial community types. It is extensible  
371 to integration of microbial community taxonomic or functional profiles from other data types (e.g.  
372 metagenomic sequencing) or environments.

373 However, all microbial community meta-analyses should be approached with caution, since in  
374 many cases unwanted sources of technical variation between studies (i.e. batch effects) are so  
375 large as to potentially mask biological signals even after correction<sup>49-51</sup> (**Supplemental Notes**).  
376 Reducing inter-study variation in microbial community profiles is challenging relative to other  
377 'omics data types due to 1) the extreme heterogeneity of microbes within most communities  
378 (exacerbating both technical and biological differences), and 2) feature zero-inflation arising from  
379 both biological and technical reasons<sup>13,52</sup>. Notably, despite these challenges, MMUPHin was able  
380 to meta-analyze amplicon profiles in this study both to associate microbial shifts with disease  
381 outcome, to associate them with treatment-specific differences, and to identify a single pattern of  
382 typical microbial variation within IBD. While previous efforts have developed IBD dysbiosis scores  
383 by contrasting patients with control groups<sup>7,9</sup>, this pattern of microbial variation was present  
384 specifically within IBD patients (both CD and UC), and in agreement with supervised methods,  
385 captured several classes of microbial functional responses in the gut (**Supplemental Note**).  
386 The IBD gut microbiome particularly stands to benefit from meta-analysis, as have other multiply-  
387 sampled conditions such as colorectal cancer<sup>53,54</sup>, in order to identify ecological and  
388 microbiological changes during the disease that are reproducible across populations. We consider  
389 this study based on 16S rRNA gene sequencing to be a proof of concept, able to achieve  
390 unprecedented power due to the number of amplicon profiled samples available, but with greater  
391 precision possible in future work using e.g. metagenomic and other 'omics technologies. This also  
392 enabled comparison of responses in the stool versus mucosal microbiomes, the latter of which  
393 are not amenable to metagenomic profiling from biopsies; these were in overall good agreement,  
394 but the few areas of significantly differential responses to inflammation are likely of particular  
395 immunological interest. The large sample and population sizes also provide some confidence in  
396 ruling out discrete, microbially-driven population subtypes as an explanation for CD and UCs'  
397 clinical heterogeneity. Instead, the work identified a single consistent axis of gradient microbial

398 change corresponding to increasing departures from “normal” microbiome configurations<sup>7,9,55</sup>.  
399 This pattern of consistent microbial dysbiosis can continue to be explored in further work on its  
400 functional, immunological, and clinical consequences. Overall, this study represents one of the  
401 first large-scale, methodologically appropriate, targeted meta-analysis of the IBD microbiome, and  
402 the corresponding methodology and its implementation are freely available for future meta-  
403 analyses of human-associated and environmental microbial populations.

404 **Methods**

405 **MMUPHin: a uniform statistical framework for meta-analysis of microbial community**  
406 **studies**

407 We developed MMUPHin (Meta-analysis Methods with a Uniform Pipeline for Heterogeneity in  
408 microbiome studies) as a framework for meta-analysis of microbial community studies using  
409 taxonomic, functional, or other abundance profiles. It includes components for batch effect  
410 adjustment, differential abundance testing, and unsupervised discrete and continuous population  
411 structure discovery.

412 Batch adjustment

413 For microbial community batch correction, we extended the batch correction method developed  
414 for gene expression data in ComBat<sup>15</sup> with an additional component to allow for the zero inflated  
415 nature of microbial abundance data. In our model, sample read count  $Y$  was modelled with respect  
416 to both batch variable and biologically relevant covariate(s)  $X$ :

417 
$$Y_{ijp} = \exp\{\beta_p X_{ij}' + \sigma_p(\gamma_{ip} + \delta_{ip}\epsilon_{ijp})\} \times I_{ijp}$$

418 Where  $i$  indicates batch/study,  $j$  indicates sample, and  $p$  indicates feature.  $\gamma_{ip}$  and  $\delta_{ip}$  are batch-  
419 specific location and scale parameters.  $\sigma_p$  is a feature-specific standardization factor.  $\beta_p$  are  
420 covariate-specific coefficients, and  $\epsilon_{ijp}$  is an independent error term following a standard normal  
421 distribution.  $I_{ijp}$  is a binary (0, 1) zero-count indicator, to allow for zero inflation of features. As in  
422 ComBat,  $\gamma_{ip}$  and  $\delta_{ip}$  are modelled with normal and inverse-gamma priors, respectively.  
423 Hyperparameters are estimated with empirical Bayes estimators as in ComBat<sup>15</sup>. The posterior  
424 means,  $\widehat{\gamma}_{ip}^*$  and  $\widehat{\delta}_{ip}^*$ , along with standard frequentist estimates  $\widehat{\beta}_p$  and  $\widehat{\sigma}_p$  are used to provide  
425 batch-corrected count data:

$$426 \quad \widetilde{Y_{ijp}} = \exp\left\{\frac{Y_{ijp} - \widehat{\beta}_p X_{ij} - \widehat{\gamma}_{ip}^* \widehat{\sigma}_p}{\widehat{\delta}_{ip}^*} + \widehat{\beta}_p X_{ij}\right\} \times I_{ijp}$$

427 Per-sample feature counts are then re-normalized to keep sample read depth unchanged post-  
428 correction. In practice, the user provides sample microbial abundance table ( $Y$ ), batch/study  
429 information, and optionally any other covariates  $X$  that are potentially confounded with batch but  
430 encode important biological information. MMUPHin outputs an adjusted profile  $\widetilde{Y}$  that is corrected  
431 for the effect of batches but retains the effects of  $X$  (if provided).

#### 432 Meta-analysis differential abundance testing

433 For meta-analytical differential abundance testing, after batch correction, MMUPHin first performs  
434 multivariate linear regression within individual studies using previously validated data  
435 transformation and modelling combinations appropriate for microbial community profiles  
436 (MaAsLin2<sup>33</sup>). This yields study-specific, per-feature differential abundance effects estimations  
437  $\widehat{\beta}_{ip}$ , where  $i$  indicates study and  $p$  indicates feature. These are then aggregated into meta-  
438 analysis effect size with fixed/random effects modelling as implemented in the metafor R  
439 package<sup>34</sup>:

440

$$\widehat{\beta}_{ip} = \beta_p + \epsilon_{ip} + e_{ip}$$

441  $\beta_p$  is the overall differential abundance effect of feature  $p$ .  $\epsilon_{ip}$  is per-study measurement error,  
442 and  $e_{ip}$  is study-specific random effects term (not present in fixed-effect models). In practice, the  
443 user provides a microbial community profile, study design (batch) information, the main exposure  
444 variable of interest, and optional additional covariates. If any meta-analyzed studies include  
445 repeated measures (e.g. longitudinal designs), then random covariates can also be provided and  
446 will be modelled for such studies. MMUPHin then performs MaAsLin2 regression modelling within  
447 each study and aggregates effect sizes of the exposure variable  $\widehat{\beta}_{ip}$  across studies using the  
448 resulting random/fixed effects model. The estimated overall effect,  $\widehat{\beta}_p$ , is reported as the overall  
449 differential abundance effect for feature  $p$ .

450 Unsupervised discrete structure discovery

451 For unsupervised discrete (i.e. cluster) structure discovery of a single study, again after batch  
452 correction, MMUPHin uses average prediction strength<sup>41</sup>, an established clustering strength  
453 metric, to measure the existence of reproducible clusters among meta-analyzed datasets. Briefly,  
454 for each individual dataset, the metric randomly and iteratively divides samples into “training” and  
455 “validation” subsets. In each iteration, clustering is first performed on the training samples, across  
456 a range of cluster numbers  $k$ , yielding (for a specific  $k$ ) training sample clusters  $A_{k1}, A_{k2}, \dots, A_{kk}$ .  
457 Note that  $A_{k1}, A_{k2}, \dots, A_{kk}$  jointly forms a partition of the testing sample indices. The same  
458 clustering analysis is then performed on the validation samples, and the resulting partition of  
459 sample space provides classification membership potentially different from clustering  
460 memberships  $A_{k1}, A_{k2}, \dots, A_{kk}$ . Prediction strength for  $k$  clusters is defined as

461  $ps(k)$

$$462 = \min_{1 \leq l \leq k} \frac{1}{n_{kl}(n_{kl} - 1)} \sum_{j \neq j' \in A_{kl}} I\{\text{validation samples } j \text{ and } j' \text{ are classified to the same group according to training samples in cluster } l\}$$

463 i.e. the minimum (across validation clusters) proportion of same-cluster sample pairs also being  
464 classified as the same group by training samples.  $n_{kl} = |A_{kl}|$ , or the number of test samples in  
465 the  $l$ th cluster.

466 Average prediction strength is the average of prediction strengths across randomization iterations.  
467 Intuitively, it characterizes the degree of agreement between the clustering structures in randomly  
468 partitioned validation and training subsets; if  $k$  is appropriately describing the true number of  
469 discrete clusters in the dataset, then average prediction strength should be close to one (training  
470 and validation samples agree most of the time).

471 We additionally generalized this metric to meta-analysis settings, where we aimed to quantify the  
472 agreement of clustering structures between studies. In the meta-analytical setting, generalized  
473 prediction strength for cluster number  $k$  in study  $i$  with validation study  $i'$  is

474  $gps_{ii'}(k)$

$$475 = \min_{1 \leq l \leq k} \frac{1}{n_{ki;l}(n_{ki;l} - 1)} \sum_{j \neq j' \in A_{ki;l}} I\{\text{validation samples } i'j \text{ and } i'j' \text{ are classified to the same group according to study } i\}$$

476 Where  $A_{kil}$  indicates the  $l$ -th cluster membership in study  $i$ , when cluster number is specified as  
477  $k$ ;  $n_{kil} = |A_{kil}|$ . The average generalized prediction in study  $i$  for cluster number  $k$  is then defined  
478 as the average of  $gps_{ii'}(k)$  across all  $i' \neq i$ , i.e., all validation studies (instead of iterations of  
479 randomized partitions). Similar to the single study prediction strength, it describes the  
480 generalizability of clustering structure in study  $i$  in external validation studies.

481 Unsupervised continuous structure discovery

482 We extended our previous work in cancer gene expression subtyping<sup>35</sup> to perform unsupervised  
483 continuous structure discovery in microbial community profiles. Complementary to discrete cluster  
484 discovery, the goal is to identify strong feature covariation signals (gradients) that are reproducible  
485 across studies. This is carried out by performing principal component analysis individually in  
486 microbiome studies and constructing a network of correlated PCA loading vectors, to identify  
487 loadings that are consistently present across studies. In detail, given a collection of training  
488 microbial abundance datasets, our method takes the following steps (visualized in **Supplemental**  
489 **Fig. 4**):

- 490 1. For each dataset  $i$ , PCA is performed on normalized and arcsin square root-transformed  
491 microbial abundance data. Given a user-specified threshold on variance explained, we  
492 record its top PC loading vectors,  $w_{i1}, w_{i2}, \dots, w_{iJ_i}$ , where  $J_i$  is the smallest number of top  
493 loading vectors that jointly explain percentage of variability in the dataset past a  
494 customizable threshold  $0 < \text{threshold}_v < 1$  (default to 80%).
- 495 2. For two PC loadings from different datasets  $w_{ij}$  and  $w_{i'j'}$ , similarity is quantified with the  
496 absolute value of cosine coefficient<sup>56</sup>  $|\cos < w_{ij}, w_{i'j'} >|$ . This yields a network of PC  
497 loading vectors associated by weighted edges  $w_{ij}$  and  $w_{i'j'}$ , retaining edges only if their  
498 weight surpasses a customizable similarity threshold ( $|\cos < w_{ij}, w_{i'j'} >| >$   
499  $\text{threshold}_s, 0 < \text{threshold}_s < 1$ ).
- 500 3. In the resulting network, we perform community detection<sup>57</sup> to identify densely connected  
501 modules of PCs. Each module by definition consists of PCs from different datasets that  
502 are similar to each other - whether or not they occur in the same order or with similar  
503 percent variance explained - and which thus represent strong feature covariation signals  
504 that are recurrent in studies.

505 4. For a module  $k$  containing PC set  $M_k$ , its consensus vector  $W_k$  is calculated as the  
506 average of sign-corrected loading vectors in  $M_k$ , i.e.,  $W_k := \frac{\sum_{w_{ij} \in M_k} \widetilde{w_{ij}}}{|M_k|}$ . Note that the  
507 average is taken not over the original loading vectors  $w_{ij}$ , but rather their sign-corrected  
508 versions  $\widetilde{w_{ij}}$ . Specifically, the signs of each  $w_{ij}$  in  $M_k$  are corrected so that all of the  
509 loading vectors have positive cosine coefficients.

510 5. The module-wide consensus vectors  $W_k$  represent strong, mutually independent, and  
511 reproducible covariation signals across the microbial datasets; they are used to identify  
512 continuously varying gradients in microbial abundance profiles that represent reproducible  
513 population structures. Specifically, given a sample with normalized and transformed  
514 microbial abundance measurements  $x$ , its continuous score for module  $k$  is defined as  
515  $x'W_k$ , as in regular PCA.

516 6. If additional studies are available, the reproducibility of each  $W_k$  can be further examined  
517 by correlating  $W_k$  with the top PC loadings in each such validation study. For each  
518 additional study,  $W_k$  is considered to be validated in that dataset if its absolute cosine  
519 coefficient with at least one of the dataset's top PCs surpasses the coefficient similarity  
520 cutoff  $threshold_s$ ; the number of top PCs to consider in the validation dataset loadings is  
521 determined with the same cutoff  $threshold_v$ .

## 522 **Simulation validation of MMUPHin**

523 We performed extensive simulation studies (**Fig. 2, Supplemental Fig. 5-8, Supplemental Table**  
524 **2**) to validate the performance of each component of MMUPHin. In all cases these employed  
525 realistic microbial abundance profiles generated using SparseDOSSA  
526 (<http://huttenhower.sph.harvard.edu/sparsedossa>). This is a model of microbial community  
527 structure using a set of zero-inflated log-normal distributions fit to selected training data, in this  
528 case drawn from the IBD gut microbiome<sup>6</sup>. Controlled microbial associations with simulated

529 covariates can then (optionally) be spiked in. Note that although the assumed null distributions in  
530 MMUPHin and SparseDOSSA are the same (zero-inflated log normal), the models of effects for  
531 batch and biological variables are substantially different: MMUPHin assumes exponentiated  
532 effects, while SparseDOSSA assumes re-standardized linear effects.

533 Specifically, SparseDOSSA models null microbial feature abundances using a zero-inflated log-  
534 normal distribution:

$$535 \quad \log(Y_{ip}) \sim N(\mu_p, \sigma_p^2) \times Bernoulli(\pi_p)$$

536 This is the same initial distributional assumption as the MMUPHin batch correction model, when  
537 there are no batch or covariates effects. However, for spiked-in associations with metadata (batch,  
538 biological variables, etc.), SparseDOSSA uses a different model. Given a simulated, pre-spiking-  
539 in feature count vector  $Y_p$  with mean  $\mu_p^Y$  and standard error  $\sigma_p^Y$ , as well as a metadata variable  
540 vector  $X$  with mean  $\mu^X$  and standard error  $\sigma^X$ , the post-spiked-in feature count is set to:

$$541 \quad \widetilde{Y_{ip}} = \frac{1}{1+\phi} \{Y_{ip} + \phi \times [\frac{(x_i - \mu^X)\sigma_p^Y}{\sigma^X} + \mu_p^Y]\}$$

542 where  $\phi$  is a configurable spike-in strength parameter. By this definition, microbial features post-  
543 spike-in have the same mean and approximately the same variance as before, the only difference  
544 being the added association with the metadata variable(s) used. This is to ensure the counts of  
545 the modified feature are not dominated by the values of the target covariate, but instead  
546 distributed similarly to real data. The SparseDOSSA association model thus differs from  
547 MMUPHin's model in two substantial ways: i) MMUPHin's associations are defined within the  
548 exponentiated component and are thus better described as a multiplicative effect, whereas  
549 SparseDOSSA's effects are directly applied on untransformed data, and ii) SparseDOSSA  
550 additionally ensures realistic data generation with the re-standardization procedure.

551 Thus, the only component of the SparseDOSSA model that requires fitting to training data is the  
552 aforementioned zero-inflated log-normal null distribution. In our analysis, this was always PRISM<sup>6</sup>,  
553 while other parameters were specified across a wide range of combinations to simulate different  
554 application scenarios. These include the effect sizes of the associated batch and biological  
555 variables (i.e. the  $\phi$  parameter), number of batches, sample sizes, as well as dimensionality (both  
556 the total number of features and the percentage of features randomized to be associated with  
557 batch/biological variables). For each combination of simulation parameters, we performed 20  
558 random replications (i.e. running simulation/evaluation with the same parameters but different  
559 random seeds). **Supplemental Table 2** presents the full list of parameter combinations.

560 Evaluating batch adjustment

561 For evaluation of MMUPHin's batch effect adjustment component, we simulated metadata that  
562 included batch (with varying total batch numbers 2, 4, 6, 8), a binary positive control (simulated  
563 "biological" covariate), continuous positive control ("biological"), and negative control (binary, and  
564 guaranteed to be non-associated with microbial features) variables. Microbial abundance data  
565 was simulated to be associated with the batch and the two positive control variables at varying  
566 effect sizes (1, 2, 5, 10 for batch variable and fixed at 10 for positive control variables), but not  
567 with the negative control variable. We additionally varied the number of samples per batch (20 to  
568 simulate multiple-batches in a single study scenario, 100 to simulate meta-analysis with moderate  
569 sized studies and 500 to simulate large meta-analysis), total number of microbial features (n=200  
570 and 1000), as well as the percentage of features associated with metadata (5%, 10%, and 20%)  
571 (**Supplemental Table 2**).

572 Performance of batch correction methods was quantified by omnibus associations (PERMANOVA  
573 R2) between the simulated microbial abundance data with the batch and positive control variables,  
574 before and after batch correction. For ComBat<sup>15</sup> and our method, batch correction was performed

575 with both positive control variables as well as the negative control variable as covariates.  
576 MMUPHin successfully reduced the confounding batch effect, but retained the effect of positive  
577 control variables, and did not inflate the effect of negative control variable (**Fig. 2a, Supplemental**  
578 **Fig. 5**).

579 Evaluating meta-analytic differential abundance testing

580 We evaluated false positive rates (FPR) in particular for meta-analytic feature association testing,  
581 specifically the null case in which there are no associations between microbial features and  
582 covariates, but false associations can arise in the presence of batch effects with unbalanced  
583 distribution of covariate values across studies (**Fig. 2b**). For simulation, we generated a binary  
584 covariate unevenly distributed between two “studies” at varying levels of disparity (**Supplemental**  
585 **Table 2**). Microbial abundance data was simulated to be associated only with the two studies and  
586 not with the covariate (i.e. study confounded null data), with varying strengths of batch effect (from  
587 0 to 10). The number of samples per batch varied between 100 and 500 to, again, simulate  
588 moderate- and large-sized meta-analysis. Lastly, we varied total number of microbial features and  
589 the percentage of features associated with metadata as above.

590 FPRs were calculated as the percentage of simulated microbial features with nominal p-values <  
591 0.05 for associations with the exposure variable. Four data normalization and analysis regimes  
592 were evaluated (**Fig. 2c, Supplemental Fig. 6**): a) naive MaAsLin2 model on the study effect  
593 confounded null data (without explicitly modelling the batches), b) the quantile normalization  
594 procedure, paired with two-tailed Wilcoxon tests, as proposed in <sup>18</sup>, c) BDMMA as proposed in <sup>19</sup>,  
595 with the default 1,0000 total MCMC sampling and 5,000 burn-in, d) the complete MMUPHin meta-  
596 analysis model for the batch corrected data as described above. Note that due to its computational  
597 cost we were only able to evaluate the Dirichlet-multinomial regression model on a subset of  
598 parameter combinations, namely number of samples per batch = 100, number of features = 200,

599 and percent of associated microbes = 5%. These parameters roughly agree with those used in  
600 the simulation analysis in the method's original publication<sup>19</sup>.

601 We also evaluated the computational costs of quantile normalization, BDMMA, and MMUPHin  
602 (**Supplemental Fig. 6**). For this, the same subset of 20 replications (batch effect 0, exposure  
603 imbalance 0, number of samples per batch 100, and number of features 200) were ran through  
604 the three methods under the same computation environment (single core Intel(R) Xeon(R) CPU  
605 E5-2680 v2 @ 2.80GHz).

606 Evaluating unsupervised discrete structure discovery

607 To simulate microbial abundance data with known discrete clustering structure, we again used  
608 the simulation model above, with microbial feature associations added both with a discrete "batch"  
609 variable and a discrete clustering variable, at varying number of batches (2, 4, 6, 8), number of  
610 clusters (3, 4, 5, 6), as well as effect size of association (0 to 10 for batch, fixed at 10 for cluster).  
611 For the evaluation of MMUPHin's unsupervised methods (both here and during continuous  
612 population structure discovery below), we fixed the number of samples per batch at 500, the  
613 number of total features at 1,000, and the percent of associated features at 20%. These were  
614 guided by the fact that the underlying unsupervised methods (clustering, PCA) require larger  
615 sample sizes for good performance even without batch confounding, and are generally only  
616 practical with higher feature dimensions (**Supplemental Table 2**).

617 Performance of clustering was evaluated as the percentage of replicates in which the right number  
618 of synthetically defined underlying clusters was identified using prediction strength, across  
619 technical replicates for a fixed combination of simulation parameters. That is, the number of  
620 clusters within a simulation was identified as that which maximized prediction strength. This was  
621 compared to the "truth" (i.e. the known simulation parameter) and counted as a success only if  
622 the two agreed. The percentage of success for a given parameter combination across the 20

623 random replications was used as the evaluation metric for model performance. We compared the  
624 performance of clustering before and after MMUPHin batch correction (**Fig. 2e, Supplemental**  
625 **Table 7**). Note that batch correction is modelled only using the batch variable and specifically not  
626 including the cluster variable as a covariate in the batch correction model above, as the underlying  
627 cluster structure is unknown in non-synthetic unsupervised analyses settings.

628 Evaluating unsupervised continuous structure discovery

629 To simulate microbial abundance data with known continuously variable population structure, we  
630 spiked in feature associations with both a simulated batch covariate (4, 6, 8) and a continuously  
631 varying gradient (uniformly distributed between -1 and 1), at varying number of batches and effect  
632 size of both associations (as above). The number of samples per batch, total number of microbial  
633 features, and the percentage of features associated were fixed at the same values as above  
634 (**Supplemental Table 2**).

635 Performance of continuous structure discovery analysis was evaluated as the Spearman  
636 correlation between the known simulated gradient score and the strongest continuously valued  
637 population structure as identified by MMUPHin's continuous structure discovery method (above).  
638 We again compared the performance of continuous score discovery on the batch confounded and  
639 batch corrected data (**Fig. 2g, Supplemental Fig. 8**). Note that, as above, batch correction is  
640 again modelled only using the batch variable and does not have any access to the synthetic  
641 continuous gradient, as any underlying continuous population structure is unknown during  
642 unsupervised analyses settings.

643 **Collection and uniform processing of ten IBD microbiome studies employing 16S rRNA**  
644 **gene sequencing**

645 Study inclusion and raw sequence data

646 We curated 10 published 16S rRNA gene sequencing (abbreviated 16S) gut microbiome studies  
647 of IBD for meta-analysis (**Table 1, Supplemental Table 1**). Demultiplexed raw sequences were  
648 either downloaded from EBI (Jansson-Lamendella and Herfarth) or available locally as previously  
649 generated (other eight studies). Metadata were obtained either directly from the sequence  
650 repository/manuscript (Herfarth, Jasson-Lamendella, HMP2, MucosalIBD, PROTECT, RISK), or  
651 from collaborators (BIDMC-FMT, CS-PRISM, LSS-PRISM, Pouchitis). This resulted in a total of  
652 5,151 samples and 2,179 subjects available prior to processing and quality control.

653 Metadata curation

654 We manually curated subject- and sample-specific metadata across studies to ensure  
655 consistency. Variables collected and curated include:

- 656 • Disease (CD, UC, control), universally available.
- 657 • Type of controls (non-IBD, healthy). Control information was available directly for CS-  
658 PRISM, Jansson-Lamendella, and Pouchitis, inferred from study design described in  
659 manuscript for Herfarth, HMP2, MucosalIBD, and RISK (all non-IBD controls), and not  
660 applicable for BIDMC-FMT, LSS-PRISM, and PROTECT (only has IBD subjects).
- 661 • Sample type (biopsy, stool), universally available.
- 662 • Body site of biopsy sample collection (ileum, colon, rectum), with more detailed  
663 classifications recorded separately in case of need. Mappings for the relevant datasets  
664 are:

665           ○ CS-PRISM: terminal ileum, neo-ileum, pouch are aggregated as ileum; cecum,  
666            ascending/left-sided colon, transverse colon, descending/right-sided colon,  
667            sigmoid colon were aggregated as colon; rectum classification was kept  
668            unchanged.

669           ○ HMP2: ileum classification kept unchanged; cecum, ascending/right-sided colon,  
670            transverse colon, descending/left-sided colon, and sigmoid colon were aggregated  
671            as colon.

672           ○ MucosalIBD: all terminal ileum samples, aggregated to ileum.

673           ○ Pouchitis: terminal ileum, pouch, pre-pouch ileum aggregated as ileum; sigmoid  
674            colon aggregated to colon.

675           ○ PROTECT: all rectum samples, classification kept unchanged.

676           ○ RISK: terminal ileum was aggregated to ileum; rectum kept unchanged.

677       ● Montreal classifications:

678           ○ Location for CDs (L1, L2, L3, and possible combinations), available for BIDMC-  
679            FMT, CS-PRISM, Herfarth, Jansson-Lamendella, LSS-PRISM, and Pouchitis.

680           ○ Behavior for CDs (B1, B2, and B3), available for CS-PRISM, Herfath, Jansson-  
681            Lamendella, LSS-PRISM, Pouchitis, and RISK.

682           ○ Extent for UCs (E1, E2, and E3), available for CS-PRISM, Jansson-Lamendella,  
683            LSS-PRISM, Pouchitis, and PROTECT.

684       ● Age at sample collection (in years), available for BIDMC-FMT, CS-PRISM, Herfarth,  
685            HMP2, LSS-PRISM, MucosalIBD, Pouchitis, PROTECT, RISK.

686       ● Age at diagnosis (in years). Directly available for CS-PRISM, HMP2, LSS-PRISM, and  
687            Pouchitis, inferred as baseline age for PROTECT and RISK as these were new-onset  
688            cohorts.

689       ● Race (White, African American, Asian / Pacific Islander, Native American, more than one  
690            race, others). Directly available for CS-PRISM, Herfarth, HMP2, PROTECT, and RISK,

691 inferred from manuscript cohort description for Jansson-Lamendella (all Caucasian  
692 cohort).

- 693 • Gender (male/female). Available for BIDMC-FMT, CS-PRISM, Herfarth, HMP2, Jansson-  
694 Lamendella, LSS-PRISM, MucosalIBD, Pouchitis, PROTECT,  
695 • Treatment variables, including antibiotics, immunosuppressants, steroids, and 5-ASA.  
696 These variables were encoded as yes/no to indicate, approximately, currently receiving  
697 them at the time of sampling. Additional information such as specific medication or delivery  
698 method was recorded separately if available in case of need. We note the potentially  
699 confounding difference in studies' definitions of treatment: for Pouchitis and PROTECT  
700 authors defined antibiotics as receiving the treatment within the past month (30 days for  
701 Pouchitis, 27 days for PROTECT), whereas for CS-PRISM, HMP2, LSS-PRISM, and RISK  
702 such determination was not possible (antibiotics "yes" was defined as "currently taking").  
703 Likewise, we had no additional information to determine the time extent for the other three  
704 treatments, beyond that according to metadata/publication, patients were "currently taking"  
705 the treatment at sample collection.

706 For a comprehensive list of curation mapping schema, please refer to our metadata curation  
707 repository: [https://github.com/biobakery/ibd\\_meta\\_analysis](https://github.com/biobakery/ibd_meta_analysis).

708 16S amplicon sequence bioinformatics and taxonomic profiling

709 Sequences were processed, per-cohort, with the published, standardized bioBakery workflow<sup>58</sup>  
710 using the UPARSE protocol<sup>59</sup> (version v9.0.2132-64bit). For all studies, demultiplexed sequences  
711 were truncated at 200bp max length and filtered by maximum expected error of one<sup>59</sup>. Operational  
712 taxonomic units (OTUs) were clustered at 97% identity and aligned using USEARCH with 97%  
713 identity to the Greengenes database 97% reference OTUs (version 13.8)<sup>60</sup> for taxonomy  
714 assignment. The resulting Greengenes identifiers for OTUs were used as basis for matching  
715 features (taxa) among cohorts.

716 Quality control

717 Across samples, a median of 81.51% reads / sample passed quality control filtering and were  
718 successfully assigned to OTUs with Greengenes identifiers (**Supplemental Fig. 1**). These 8,921  
719 raw OTUs aggregated to a total of 1,122 genera prior to quality control. We retained taxa that  
720 exceeded 5e-5 relative abundance with at least 10% prevalent in at least one study; this criterion  
721 generally removes spurious OTU assignments while retaining rare organisms if confidently  
722 present in at least one study. Lastly, we also removed low read depth samples with less than  
723 3,000 total sequences, which retained 78.34%-100% samples per cohorts (**Supplemental Table**  
724 **1**). The final resulting taxonomic profile, used for all further analysis, aggregated into 249 total  
725 genera spanning 4,789 samples (OTUs unclassified under a particular taxonomy level were  
726 aggregated as “unclassified” feature under that taxon, e.g. “Enterbacteriaceae unclassified”  
727 accumulates all OTUs’ abundances under the family that could not be classified at the genus level.

728 Data availability

729 Quality controlled (truncated and filtered) sequences, Greengenes mapped OTU count profiles,  
730 and curated sample metadata are available at the Human Microbial Bioactives Resource Portal  
731 (<http://portal.microbiome-bioactives.org>).

732 **Applying MMUPHin to IBD gut microbiome meta-analysis**

733 For the resulting collection of microbiome studies, batch and study effects was performed using  
734 MMUPHin on both the genus level feature abundance profiles. For either taxonomic rank, batch  
735 (i.e., sequencing run) effect correction was first performed within individual studies (when  
736 batch/plate information was available, applicable to BIDMC-FMT, CS-PRISM, LSS-PRISM,  
737 MucosalIBD, and RISK). Microbial abundance profiles across all studies were then jointly  
738 corrected for study effects, while modelling disease status (IBD or control), disease (CD or UC),

739 and sample type (biopsy or stool) as covariates. Reduction of batch and study effects was  
740 evaluated by PERMANOVA R2 (**Fig. 3a**).

741 **Association analyses**

742 Omnibus testing of microbial composition associations

743 We used PERMANOVA tests (2,000 permutations) as implemented in the R package vegan<sup>37</sup>  
744 using Bray-Curtis dissimilarities for all omnibus association tests of overall microbial community  
745 structure with covariates (**Fig. 3a**). Where appropriate, R2s were calculated conditioning on the  
746 necessary covariates; specifically, CD/UC Montreal classifications were conditional on CD/UC  
747 samples respectively, treatment was conditional on IBD status, biopsy location was conditional  
748 on a sample being a biopsy, and all covariates were conditional on being non-missing. Otherwise,  
749 variables were tested marginally (that is, each as the sole variable in the model). Importantly, to  
750 account for repeated measures within subjects for longitudinal studies, we adopted the blocked  
751 permutation strategy as in <sup>9</sup>, where per-sample measurements (sample type, biopsy location,  
752 treatment) were permuted within subjects, and per-subject measurements (disease,  
753 demographics) were permuted along with subjects (but within cohorts, relevant for the all-cohorts  
754 evaluation). For a full list of the model and permutation strategies that this resulted in for our  
755 analysis, please refer to **Supplemental Table 3**. Finally, per-variable p-values were adjusted with  
756 Benjamini-Hochberg false discovery rate control on a per-study basis.

757 Per-feature meta-analysis differential abundance testing

758 To identify microbial features individually significantly associated with one or more covariates, we  
759 applied MMUPHin's differential abundance testing model as described above. Cohorts were first  
760 stratified by sample type (biopsy or stool) and, where appropriate, diseases (CD or UC) prior to  
761 model fitting. Arcsin square root-transformed genus level taxon abundances were tested for

762 covariate associations in individual cohort strata with multivariate linear modelling (linear random  
763 intercept model adopted for longitudinal studies). Covariates used for adjustment include age,  
764 gender, and race for disease variables, and additionally disease status for treatment variables.  
765 Effect sizes across cohort strata were aggregated with a random effects model with restricted  
766 maximum likelihood estimation<sup>34</sup>. P-values were FDR adjusted across features for each variable.  
767 For the full list of models adopted as well as cohort stratification strategy, please refer to  
768 **Supplemental Table 3**. **Fig. 3b** visualizes the aggregated meta-analysis effects; for individual  
769 study results refer to **Supplemental Table 4**.

770 Testing for phenotypic severity within CD and UC patients

771 Meta-analytical testing of features associated with CD behavior and UC extent classifications  
772 were performed with similar models (**Supplemental Table 3**). Specifically, within each study's  
773 CD patients, the tests for contrasts B2 versus B1 and B3 versus B1 are performed by  
774 Relative abundance  $\sim \beta_0 + \beta_1 I\{\text{subject is B2}\} + \text{additional covariates}$  (subsetted to B1, B2 CDs)  
775 Relative abundance  $\sim \beta_0 + \beta_1 I\{\text{subject is B3}\} + \text{additional covariates}$  (subsetted to B1, B3 CDs)  
776 The two  $\beta_1$  coefficients, once aggregated with meta-analysis, were reported as the effect sizes  
777 shown in **Fig. 4a**, along with their FDR corrected q-values (adjusted across features for each  
778 test).

779 Relative abundance  $\sim \beta_0 + \beta_1 I\{\text{subject is B2 or B3}\} + \beta_2 I\{\text{subject is B3}\} + \text{additional covariates}$   
780  $\beta_2$  in this model corresponds to the effect of B3 in addition to the overall contrasts between B23  
781 versus B1. The meta-analysis aggregated p-values of these effects were reported as the  
782 differentiation between the most severe and “medium” severity phenotypes (vertical bars  
783 indicating significance in **Fig. 4a**). Note that FDR adjustment of this effect was performed across  
784 the subset of features with at least either B2 versus B1 or B3 versus B1 effect significant (i.e., the

785 subset of features visualized in **Fig. 4a**). Equivalent models were adopted for contrasts between  
786 extent categories of UC patients. Individual study results for the aggregated effects in **Fig. 4a** are  
787 in **Supplemental Table 5**.

788 Interaction effects testing

789 To test for interaction effects with sample type and diseases, we fit meta-analysis moderator  
790 models<sup>34</sup> on the per cohort strata effects:

791 
$$\widehat{\beta_{ip}} = \beta_{0p} + \beta_{1p}I\{\text{cohort strata } i \text{ is biopsy}\} + \epsilon_{ip} + e_{ip}$$

792 
$$\widehat{\beta_{ip}} = \beta_{0p} + \beta_{1p}I\{\text{cohort strata } i \text{ is CD}\} + \epsilon_{ip} + e_{ip}$$

793 The moderator effects  $\beta_{1p}$  correspond to the interaction effect between the exposure under  
794 evaluation (disease, treatment, etc.) with the moderator variable. **Fig. 4b** visualizes the two  
795 example features, *Dehalobacterium* and *Enterobacteriaceae*; all significant interactions as well as  
796 individual study effects are in **Supplemental Table 6**.

797 **Population structure analyses**

798 Discrete structure discovery

799 We performed discrete subtype discovery (i.e. “enterotyping”<sup>61</sup>) in IBD, CD, and UC populations  
800 across studies (longitudinal studies subsetted to baseline samples), using MMUPHin’s discrete  
801 structure discovery component. Only studies with at least 33 samples were considered for  
802 clustering analysis, as this was the sample size in the original enterotype paper<sup>26</sup>. Specifically,  
803 clustering was performed on Bray-Curtis dissimilarity by the partition-around-medoid method as  
804 implemented in R package cluster; the same method was adopted in previous enterotyping efforts  
805 including the original enterotype paper<sup>26,40</sup>. Clustering was evaluated with prediction strength and  
806 validated externally with MMUPHin’s generalized prediction strength as described above. Across

807 studies, we found no evidence to support a particular number of clusters within IBD, CD, or UC  
808 populations (**Fig. 5a, Supplemental Fig. 9**), suggesting that the IBD microbiome does not have  
809 discrete clusters.

810 We additionally extended our clustering evaluation analysis to other dissimilarity metrics (Jaccard,  
811 root Jensen-Shannon divergence) and clustering strength measurements (Calinski-Harabasz  
812 index, average silhouette width), which were also explored in previous efforts<sup>40</sup>. Importantly, the  
813 original enterotype paper adopted root Jensen-Shannon divergence and Calinski-Harabasz index  
814 for cluster discovery. Across combinations of these additional dissimilarities and clustering  
815 strength metrics, we also found no evidence to support discrete clusters (**Supplemental Fig. 9**).

816 Continuous structure discovery

817 Continuous structure discovery was performed with MMUPHin's corresponding component. The  
818 four largest studies (CS-PRISM, Pouchitis, PROTECT, RISK) were subsetted to baseline samples  
819 (only relevant for PROTECT), stratified by CD/UC and biopsy/stool sample type, and used as the  
820 training sets for MMUPHin. The minimum variance explained threshold ( $threshold_v$ ) was set to  
821 default (80%), but we varied the PC similarity (evaluated by absolute cosine coefficient)  
822 cutoff  $threshold_s$  between 0.5 and 0.8 to assess the sensitivity of the two identified PC clusters in  
823 **Fig. 5b** (corresponding to  $threshold_s = 0.65$ ). As we show in **Supplemental Fig. 11**, with a small  
824  $threshold_s$  (0.5) PC networks become denser, with the two PC clusters in **Fig. 4b** forming key  
825 components of two larger clusters; when  $threshold_s$  is large (0.8) the network is sparser, with  
826 only the most highly similar nodes of the two clusters forming smaller communities. We thus  
827 concluded that the two identified clusters in **Fig. 5b** were not sensitive to the cosine coefficient  
828 threshold, as they were recurrently identified in both smaller and larger cutoff scenarios.

829 Continuous structure validation

830 We validated the consistency of the two clusters' corresponding continuous scores in all IBD  
831 cohorts, non-IBD and healthy control samples, as well as a randomly permuted mock study (as a  
832 negative control). The reproducibility of each continuous score within a study was defined as the  
833 maximum absolute cosine coefficient between the score's consensus loading (as provided by  
834 MMUPHin) and the top three principal component loadings discovered independently within that  
835 study. Note that the number of top principal components considered here was set to a fixed value  
836 (three) instead of based on a percent variance cutoff as in the MMUPHin continuous structure  
837 discovery stage. This is because in the two identified clusters in **Fig. 5c**, the latest included node  
838 was PC3. The randomly permuted study consisted of 473 samples (median validation data sets  
839 sample size) randomly selected from the entire meta-analysis collection, but each sample's  
840 microbial abundance was independently permuted across features. This was to simulate a  
841 "negative control" dataset where there should be no continuous population structures.

842 As we show in **Supplemental Fig. 12**, the dysbiosis score was well validated across studies,  
843 except for healthy control samples and the negative control dataset. The Firmicutes-versus-  
844 Bacteroidetes trade-off score, on the other hand, was reasonably well reproduced in all studies  
845 and particularly well-established in healthy samples, but, again, was not significantly detected in  
846 the negative control dataset.

847 Continuous score assignment

848 Assignment of continuous scores was straightforward given the two consensus loading vectors  
849 provided by MMUPHin. Within each study, arcsin square root-transformed relative abundances  
850 were centered per-feature, the transformed abundance matrix was then multiplied by each  
851 consensus loading via dot product to generate per-sample continuous scores. These scores were  
852 used for visualization as in **Fig. 4d** and **Supplemental Fig. 10**, as well as for testing the difference

853 between CD, UC, non-IBD, and healthy control populations as in **Supplemental Fig. 13** We  
854 provide the two consensus loadings in **Supplemental Table 7**; interested researchers can follow  
855 these steps to assign the two continuous scores in other datasets.  
856

857 **References**

858 1 Hirschhorn, J. N. & Daly, M. J. Genome-wide association studies for common diseases  
859 and complex traits. *Nat Rev Genet* **6**, 95-108, doi:10.1038/nrg1521 (2005).

860 2 Lambert, J. C. *et al.* Meta-analysis of 74,046 individuals identifies 11 new susceptibility  
861 loci for Alzheimer's disease. *Nat Genet* **45**, 1452-1458, doi:10.1038/ng.2802 (2013).

862 3 Franke, A. *et al.* Genome-wide meta-analysis increases to 71 the number of confirmed  
863 Crohn's disease susceptibility loci. *Nat Genet* **42**, 1118-1125, doi:10.1038/ng.717 (2010).

864 4 Anderson, C. A. *et al.* Meta-analysis identifies 29 additional ulcerative colitis risk loci,  
865 increasing the number of confirmed associations to 47. *Nat Genet* **43**, 246-252,  
866 doi:10.1038/ng.764 (2011).

867 5 Price, A. L. *et al.* Principal components analysis corrects for stratification in genome-wide  
868 association studies. *Nat Genet* **38**, 904-909, doi:10.1038/ng1847 (2006).

869 6 Morgan, X. C. *et al.* Dysfunction of the intestinal microbiome in inflammatory bowel  
870 disease and treatment. *Genome Biol* **13**, R79, doi:10.1186/gb-2012-13-9-r79 (2012).

871 7 Gevers, D. *et al.* The treatment-naive microbiome in new-onset Crohn's disease. *Cell Host  
872 Microbe* **15**, 382-392, doi:10.1016/j.chom.2014.02.005 (2014).

873 8 Ananthakrishnan, A. N. Environmental risk factors for inflammatory bowel diseases: a  
874 review. *Dig Dis Sci* **60**, 290-298, doi:10.1007/s10620-014-3350-9 (2015).

875 9 Lloyd-Price, J. *et al.* Multi-omics of the gut microbial ecosystem in inflammatory bowel  
876 diseases. *Nature* **569**, 655-662, doi:10.1038/s41586-019-1237-9 (2019).

877 10 Willer, C. J., Li, Y. & Abecasis, G. R. METAL: fast and efficient meta-analysis of  
878 genomewide association scans. *Bioinformatics* **26**, 2190-2191,  
879 doi:10.1093/bioinformatics/btq340 (2010).

880 11 Rhodes, D. R. *et al.* Large-scale meta-analysis of cancer microarray data identifies  
881 common transcriptional profiles of neoplastic transformation and progression. *Proc Natl  
882 Acad Sci U S A* **101**, 9309-9314, doi:10.1073/pnas.0401994101 (2004).

883 12 Li, H. Microbiome, Metagenomics, and High-Dimensional Compositional Data Analysis.  
884 *Annual Review of Statistics and Its Application* **2**, 73-94, doi:10.1146/annurev-statistics-  
885 010814-020351 (2015).

886 13 Mallick, H. *et al.* Experimental design and quantitative analysis of microbial community  
887 multiomics. *Genome Biol* **18**, 228, doi:10.1186/s13059-017-1359-z (2017).

888 14 Li, Y., Willer, C., Sanna, S. & Abecasis, G. Genotype imputation. *Annu Rev Genomics  
889 Hum Genet* **10**, 387-406, doi:10.1146/annurev.genom.9.081307.164242 (2009).

890 15 Johnson, W. E., Li, C. & Rabinovic, A. Adjusting batch effects in microarray expression  
891 data using empirical Bayes methods. *Biostatistics* **8**, 118-127,  
892 doi:10.1093/biostatistics/kxj037 (2007).

893 16 Leek, J. T. & Storey, J. D. Capturing heterogeneity in gene expression studies by  
894 surrogate variable analysis. *PLoS Genet* **3**, 1724-1735,  
895 doi:10.1371/journal.pgen.0030161 (2007).

896 17 Leek, J. T. *et al.* Tackling the widespread and critical impact of batch effects in high-  
897 throughput data. *Nat Rev Genet* **11**, 733-739, doi:10.1038/nrg2825 (2010).

898 18 Gibbons, S. M., Duvallet, C. & Alm, E. J. Correcting for batch effects in case-control  
899 microbiome studies. *PLoS Comput Biol* **14**, e1006102, doi:10.1371/journal.pcbi.1006102  
900 (2018).

901 19 Dai, Z., Wong, S. H., Yu, J. & Wei, Y. Batch effects correction for microbiome data with  
902 Dirichlet-multinomial regression. *Bioinformatics* **35**, 807-814,  
903 doi:10.1093/bioinformatics/bty729 (2019).

904 20 Manichanh, C., Borruel, N., Casellas, F. & Guarner, F. The gut microbiota in IBD. *Nat Rev  
905 Gastroenterol Hepatol* **9**, 599-608, doi:10.1038/nrgastro.2012.152 (2012).

906 21 Kostic, A. D., Xavier, R. J. & Gevers, D. The microbiome in inflammatory bowel disease:  
907 current status and the future ahead. *Gastroenterology* **146**, 1489-1499,  
908 doi:10.1053/j.gastro.2014.02.009 (2014).

909 22 Halfvarson, J. *et al.* Dynamics of the human gut microbiome in inflammatory bowel disease.  
910 *Nat Microbiol* **2**, 17004, doi:10.1038/nmicrobiol.2017.4 (2017).

911 23 Schirmer, M. *et al.* Compositional and Temporal Changes in the Gut Microbiome of  
912 Pediatric Ulcerative Colitis Patients Are Linked to Disease Course. *Cell Host Microbe* **24**,  
913 600-610 e604, doi:10.1016/j.chom.2018.09.009 (2018).

914 24 Pasolli, E., Truong, D. T., Malik, F., Waldron, L. & Segata, N. Machine Learning Meta-  
915 analysis of Large Metagenomic Datasets: Tools and Biological Insights. *PLoS Comput  
916 Biol* **12**, e1004977, doi:10.1371/journal.pcbi.1004977 (2016).

917 25 Duvallet, C., Gibbons, S. M., Gurry, T., Irizarry, R. A. & Alm, E. J. Meta-analysis of gut  
918 microbiome studies identifies disease-specific and shared responses. *Nat Commun* **8**,  
919 1784, doi:10.1038/s41467-017-01973-8 (2017).

920 26 Arumugam, M. *et al.* Enterotypes of the human gut microbiome. *Nature* **473**, 174-180,  
921 doi:10.1038/nature09944 (2011).

922 27 Vazquez-Baeza, Y. *et al.* Guiding longitudinal sampling in IBD cohorts. *Gut* **67**, 1743-1745,  
923 doi:10.1136/gutjnl-2017-315352 (2018).

924 28 Morgan, X. C. *et al.* Associations between host gene expression, the mucosal microbiome,  
925 and clinical outcome in the pelvic pouch of patients with inflammatory bowel disease.  
926 *Genome Biol* **16**, 67, doi:10.1186/s13059-015-0637-x (2015).

927 29 Franzosa, E. A. *et al.* Gut microbiome structure and metabolic activity in inflammatory  
928 bowel disease. *Nat Microbiol* **4**, 293-305, doi:10.1038/s41564-018-0306-4 (2019).

929 30 Liu, T. C. *et al.* Paneth cell defects in Crohn's disease patients promote dysbiosis. *JCI  
930 Insight* **1**, e86907, doi:10.1172/jci.insight.86907 (2016).

931 31 Hall, A. B. *et al.* A novel *Ruminococcus gnavus* clade enriched in inflammatory bowel  
932 disease patients. *Genome Med* **9**, 103, doi:10.1186/s13073-017-0490-5 (2017).

933 32 Vaughn, B. P. *et al.* Increased Intestinal Microbial Diversity Following Fecal Microbiota  
934 Transplant for Active Crohn's Disease. *Inflamm Bowel Dis* **22**, 2182-2190,  
935 doi:10.1097/MIB.0000000000000893 (2016).

936 33 Mallick, H., Rahnavard, A. & McIver, L. Maaslin2: Maaslin2. R package version 1.2.0,  
937 <http://huttenhower.sph.harvard.edu/maaslin2>.  
938 *Bioconductor*, doi:10.18129/B9.bioc.Maaslin2 (2019).

939 34 Viechtbauer, W. Conducting Meta-Analyses in R with the metafor Package. *2010* **36**, 48,  
940 doi:10.18637/jss.v036.i03 (2010).

941 35 Ma, S. *et al.* Continuity of transcriptomes among colorectal cancer subtypes based on  
942 meta-analysis. *Genome Biol* **19**, 142, doi:10.1186/s13059-018-1511-4 (2018).

943 36 Huber, W. *et al.* Orchestrating high-throughput genomic analysis with Bioconductor. *Nat  
944 Methods* **12**, 115-121, doi:10.1038/nmeth.3252 (2015).

945 37 Oksanen, J. *et al.* (2019).

946 38 Vilhjalmsson, B. J. & Nordborg, M. The nature of confounding in genome-wide association  
947 studies. *Nat Rev Genet* **14**, 1-2, doi:10.1038/nrg3382 (2013).

948 39 Ravel, J. *et al.* Vaginal microbiome of reproductive-age women. *Proc Natl Acad Sci U S A  
949 108 Suppl 1*, 4680-4687, doi:10.1073/pnas.1002611107 (2011).

950 40 Koren, O. *et al.* A guide to enterotypes across the human body: meta-analysis of microbial  
951 community structures in human microbiome datasets. *PLoS Comput Biol* **9**, e1002863,  
952 doi:10.1371/journal.pcbi.1002863 (2013).

953 41 Tibshirani, R. & Walther, G. Cluster Validation by Prediction Strength. *Journal of  
954 Computational and Graphical Statistics* **14**, 511-528, doi:10.1198/106186005X59243  
955 (2005).

956 42 Wold, S., Esbensen, K. & Geladi, P. Principal component analysis. *Chemometrics and  
957 intelligent laboratory systems* **2**, 37-52, doi:10.1016/0169-7439(87)80084-9 (1987).

958 43 Satsangi, J., Silverberg, M. S., Vermeire, S. & Colombel, J. F. The Montreal classification  
959 of inflammatory bowel disease: controversies, consensus, and implications. *Gut* **55**, 749-  
960 753, doi:10.1136/gut.2005.082909 (2006).

961 44 Lin, M. F. & Lan, C. Y. Antimicrobial resistance in *Acinetobacter baumannii*: From bench  
962 to bedside. *World J Clin Cases* **2**, 787-814, doi:10.12998/wjcc.v2.i12.787 (2014).

963 45 Kevans, D. *et al.* Characterization of Intestinal Microbiota in Ulcerative Colitis Patients with  
964 and without Primary Sclerosing Cholangitis. *J Crohns Colitis* **10**, 330-337,  
965 doi:10.1093/ecco-jcc/jjv204 (2016).

966 46 Presley, L. L., Wei, B., Braun, J. & Borneman, J. Bacteria associated with  
967 immunoregulatory cells in mice. *Appl Environ Microbiol* **76**, 936-941,  
968 doi:10.1128/AEM.01561-09 (2010).

969 47 Jones-Hall, Y. L., Kozik, A. & Nakatsu, C. Ablation of tumor necrosis factor is associated  
970 with decreased inflammation and alterations of the microbiota in a mouse model of  
971 inflammatory bowel disease. *PLoS One* **10**, e0119441, doi:10.1371/journal.pone.0119441  
972 (2015).

973 48 Imhann, F. *et al.* Interplay of host genetics and gut microbiota underlying the onset and  
974 clinical presentation of inflammatory bowel disease. *Gut* **67**, 108-119, doi:10.1136/gutjnl-  
975 2016-312135 (2018).

976 49 Sinha, R. *et al.* Assessment of variation in microbial community amplicon sequencing by  
977 the Microbiome Quality Control (MBQC) project consortium. *Nat Biotechnol* **35**, 1077-1086,  
978 doi:10.1038/nbt.3981 (2017).

979 50 Brooks, J. P. *et al.* The truth about metagenomics: quantifying and counteracting bias in  
980 16S rRNA studies. *BMC Microbiol* **15**, 66, doi:10.1186/s12866-015-0351-6 (2015).

981 51 Schloss, P. D. Identifying and Overcoming Threats to Reproducibility, Replicability,  
982 Robustness, and Generalizability in Microbiome Research. *MBio* **9**,  
983 doi:10.1128/mBio.00525-18 (2018).

984 52 Tsilimigras, M. C. & Fodor, A. A. Compositional data analysis of the microbiome:  
985 fundamentals, tools, and challenges. *Ann Epidemiol* **26**, 330-335,  
986 doi:10.1016/j.annepidem.2016.03.002 (2016).

987 53 Thomas, A. M. *et al.* Metagenomic analysis of colorectal cancer datasets identifies cross-  
988 cohort microbial diagnostic signatures and a link with choline degradation. *Nat Med* **25**,  
989 667-678, doi:10.1038/s41591-019-0405-7 (2019).

990 54 Wirbel, J. *et al.* Meta-analysis of fecal metagenomes reveals global microbial signatures  
991 that are specific for colorectal cancer. *Nat Med* **25**, 679-689, doi:10.1038/s41591-019-  
992 0406-6 (2019).

993 55 Lloyd-Price, J. *et al.* Strains, functions and dynamics in the expanded Human Microbiome  
994 Project. *Nature* **550**, 61-66, doi:10.1038/nature23889 (2017).

995 56 Jaskowiak, P. A., Campello, R. J. & Costa, I. G. On the selection of appropriate distances  
996 for gene expression data clustering. *BMC Bioinformatics* **15 Suppl 2**, S2,  
997 doi:10.1186/1471-2105-15-S2-S2 (2014).

998 57 Csardi, G. & Nepusz, T. The igraph software package for complex network research.  
999 *InterJournal Complex Systems*, 1695-1695 (2006).

1000 58 McIver, L. J. *et al.* bioBakery: a meta'omic analysis environment. *Bioinformatics* **34**, 1235-  
1001 1237, doi:10.1093/bioinformatics/btx754 (2018).

1002 59 Edgar, R. C. UPARSE: highly accurate OTU sequences from microbial amplicon reads.  
1003 *Nat Methods* **10**, 996-998, doi:10.1038/nmeth.2604 (2013).

1004 60 McDonald, D. *et al.* An improved Greengenes taxonomy with explicit ranks for ecological  
1005 and evolutionary analyses of bacteria and archaea. *ISME J* **6**, 610-618,  
1006 doi:10.1038/ismej.2011.139 (2012).

1007 61 Costea, P. I. *et al.* Enterotypes in the landscape of gut microbial community composition.  
1008 *Nat Microbiol* **3**, 8-16, doi:10.1038/s41564-017-0072-8 (2018).

